

## Preparation of hybrid composite microspheres containing nanosilicon via microsuspension polymerization

Fandong Liu,<sup>1</sup> Zhoulu Wang,<sup>1</sup> Yingjie Zhou,<sup>2</sup> Xiang Liu<sup>1</sup>

<sup>1</sup>Key Laboratory of Flexible Electronics (KLOFE) & Institute of Advanced Materials (IAM), National Jiangsu Synergistic Innovation Center for Advanced Materials (SICAM), Nanjing Tech University (Nanjing Tech), 30 South Puzhu Road, Nanjing 211816, China

<sup>2</sup>School of Physics and Optoelectronic Engineering, Nanjing University of Information Science & Technology, 219 Ningliu Road, Nanjing 210044, China

Correspondence to: X. Liu (E-mail: iamxliu@njtech.edu.cn)

**ABSTRACT:** Hybrid composite microspheres with nano-Si as the core and poly(styrene-*co*-acrylonitrile) as a shell are successfully prepared by a two-step polymerization technique, which includes dispersion polymerization of styrene and 3-methacryloxypropyl trimethoxysilane in ethanol for surface modification of nano-Si followed by microsuspension polymerization of styrene and acrylonitrile in an aqueous phase for encapsulating nano-Si into an SAN copolymer matrix. The structure and surface properties of modified nano-Si are investigated by Fourier transform infrared spectroscopy (FTIR) and contact angle. The hybrid composite microspheres are systematically characterized by energy dispersive spectroscopy, thermogravimetric analysis, and transmission electron microscopy (TEM). According to the FTIR spectra and the contact angle experiments, it was determined that a hydrophobic polymer layer was formed on the surface of nano-Si. TEM showed that nano-Si was homogeneously dispersed in SAN particles when the loading capacity of nano-Si in the hybrid composite microspheres was less than 20 wt %. Moreover, scanning electron microscopy and X-ray photoelectron spectroscopy revealed that there were large amounts of nano-Si absorbed on the surface of the hybrid composite microspheres, and the mean particle size became much larger when the loading amounts of nano-Si reached 25 wt %. From this, it can be inferred that nano-Si overflows from the inner core to the outside surface in the emulsification process and acts as an inorganic dispersant. © 2015 Wiley Periodicals, Inc. *J. Appl. Polym. Sci.* **2016**, *133*, 43101.

**KEYWORDS:** copolymers; radical polymerization; surfaces and interfaces

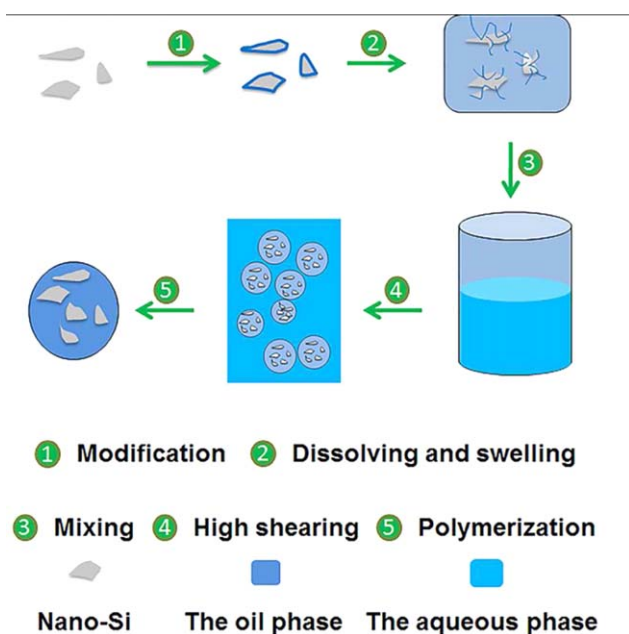
Received 26 May 2015; accepted 25 October 2015

DOI: 10.1002/app.43101

### INTRODUCTION

Silicon is a promising anode material used for lithium-ion batteries because of its much higher theoretical specific capacity (4200 mAh g<sup>-1</sup>).<sup>1-3</sup> It is known that nano-Si agglomeration is a significant barrier in the practical application of silicon-based electrode materials because of its high surface energy.<sup>4,5</sup> Therefore, many endeavors have been attempted to solve this problem, including assembling ultrafine Si anode materials into continuous film structures,<sup>6,7</sup> using Si-based nanowires,<sup>8,9</sup> constructing three-dimensional nanoporous Si frameworks,<sup>10,11</sup> preparing carbon-coated Si nanocomposites, and depositing Si on a carbon substrate.<sup>5,12,13</sup> Among all the reported nanostructures, the most effective way is to create nanocomposites composed of nano-Si uniformly embedded in the carbon matrix.<sup>15,16</sup> Carbon coatings are attractive because carbon as a structural buffer is not only lightweight, but also has a small volume effect and good electrical conductivity.<sup>11,17</sup> For example, Ng *et al.* reported amorphous carbon-coated Si nanocomposites in which the car-

bon coating exhibited the beneficial effect of enhancing the dimensional stability of the Si nanoparticles.<sup>18</sup> Moreover, a carbon-coated Si/graphene nanocomposite was prepared by dispersing a mixture containing graphene,<sup>12</sup> citric acid, and Si nanoparticles in ethanol. Transmission electron microscopy revealed that a carbon layer with a uniform thickness was formed on the surface of the Si nanoparticles with the graphene addition.<sup>19,20</sup> Recently, several researchers have shown interest in Si hybrid nanocomposites prepared by polymerization because more homogeneously dispersed nanocomposites can be obtained by increasing the interfacial interactions between two components via the formation of hydrogen bonds or covalent bonds.<sup>21-24</sup> Zhang *et al.* presented an effective approach for the synthesis of a core-shell Si hybrid nanocomposite prepared by emulsion polymerization.<sup>25</sup> They have claimed that the nanocomposite with polyacrylonitrile (PAN) as a shell and Si nanoparticles as the core could be applied successfully to Si-based electrode materials.<sup>26,27</sup> In addition, Kwon *et al.* showed that



**Scheme 1.** The synthetic route of SAN-Si hybrid composite microspheres. [Color figure can be viewed in the online issue, which is available at [wileyonlinelibrary.com](http://wileyonlinelibrary.com).]

Ag-deposited Si/poly(acrylonitrile-*co*-3-methacryloxypropyl trimethoxysilane) multicore/shell microspheres were synthesized by suspension polymerization.<sup>28</sup> They dispersed silicon nanopowders in a methylene chloride solvent with mechanical stirring and sonication and subsequently mixed them with monomers to polymerize. However, it is often impossible to redisperse silicon nanopowders into individual nanoparticles through the ultrasonic method, due to their small size and extremely high surface energy.

In this study, a new strategy for surface modification of nano-Si prepared from high-energy wet ball milling by dispersion copolymerization of 3-methacryloxypropyl trimethoxysilane (TMPTS) and styrene is developed so that the nano-Si could be homogeneously embedded in polymer microspheres (Scheme 1).<sup>29,30</sup> In comparison with nano-Si pretreated by TMPTS alone, dispersion copolymerization of TMPTS and styrene is more effective for improving the dispersion of nano-Si and compatibility with the polymer matrix.<sup>31,32</sup> Then microsuspension polymerization of styrene and acrylonitrile in an aqueous phase has been successfully carried out to encapsulate modified nano-Si into poly(styrene-*co*-acrylonitrile) (SAN) particles. The resulting hybrid composite microspheres, characterized by microscopy techniques, exhibited well-dispersed nano-Si up to loadings as high as 20 wt %, beyond which surface agglomeration was observed.

## EXPERIMENTAL

### Materials

Styrene (St; analytical grade from Aldrich, Shanghai, China) and acrylonitrile (AN; analytical grade from Aldrich) were distilled under reduced pressure to remove inhibitors and kept at 0°C before use. Benzoyl peroxide (BPO; 70%), poly(vinyl alco-

hol) (PVA;  $M_w = 85\text{--}146$  kDa, degree of hydrolysis 87–89%), polyoxyethylene alkyl ether sulfate, and sodium nitrite ( $\text{NaNO}_2$ ; 99%), all from Aldrich, were used as initiator, stabilizer, costabilizer, and inhibitor, respectively, without any further purification. Distilled water was used as the continuous phase. The coupling agent, TMPTS, was purchased from Acros Organics (Acros Organics USA Ltd, Belgium, USA) and used as received. The chain transfer agent, T-dodecyl mercaptan (TDM) was used without further treatment. Commercial micrometric silicon powder (99.9%, 1–5 micron, Alfa Aesar, Ward Hill, MA, United States) was used as raw material.

### Preparation of Nano-Si Dispersion Solution

The silicon powder was mixed with ethanol with a mass ratio of 1:9 in a 500 mL holding tank and stirred vigorously for 30 min to form uniform mixtures, which were then introduced into a ball mill with a zirconia grinding chamber of approximately 160 mL containing 140 mL (apparent volume) zirconia balls (diameter 0.8 mm). The rotating speed was adjusted to 3800 rpm.<sup>29</sup>

### Surface Modification of Nano-Si

The new strategy for the surface modification of nano-Si was employed as follows. Monomer mixtures of St (25 g), TMPTS (12.5 g), BPO (1.07 g), and chain transfer agent TDM (1.88 g) were added into a nano-Si dispersion solution (234 g, 10.7 wt %) obtained from high-energy wet ball milling. The mixtures were then heated in a 500 mL glass reactor equipped with a reflux condenser under a slow stream of  $\text{N}_2$  for 12 h at 73°C. Finally, the surface of nano-Si was partially covered with segments or oligomers, mainly due to the nanoeffect and the reaction between free —OH groups of nano-Si and TMPTS. The modified nano-Si was extracted with toluene to remove the ungrafted TMPTS-*co*-St completely. The grafting ratio ( $f_r$ ) and efficiency ( $f_e$ ) of TMPTS-*co*-St were calculated as follows<sup>33</sup>:

$$f_r = \frac{M_C - (M - M')}{M_{\text{Si}}} \times 100\% \quad (1)$$

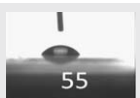
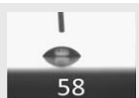

$$f_e = \frac{M_C - (M - M')}{M_C} \times 100\% \quad (2)$$

where  $M_{\text{Si}}$  is the mass of pristine nano-Si added,  $M$  is the mass of modified nano-Si before Soxhlet extraction,  $M'$  is the mass of modified nano-Si after Soxhlet extraction, and  $M_C$  is the mass of TMPTS-*co*-St formed.

### Synthesis of Poly(styrene-*co*-acrylonitrile)-silicon Hybrid Composite Microspheres

Poly(styrene-*co*-acrylonitrile)-silicon (SAN-Si) hybrid composite microspheres were prepared via microsuspension polymerization.<sup>34,35</sup> St (70 g) was mixed with the modified nano-Si with various Si contents (5 g, 10 g, 15 g, 20 g, and 25 g, denoted as SAN-Si5, SAN-Si10, SAN-Si15, SAN-Si20, and SAN-Si25, respectively), followed by the evaporation of ethanol from the system under reduced pressure at room temperature. The nano-Si could be well dispersed in St monomer because the surface of the nano-Si was partially covered with hydrophobic polymer layers. AN (30 g) and BPO (4 g) were added into the above mixtures, and then they were mixed with 0.67 wt % PVA aqueous solution (450 g), containing polyoxyethylene alkyl ether

**Table I.** Influence of the Modification Methods of Nano-Si on  $f_n$ ,  $f_o$ , and Water Contact Angle

Sample	Nano-Si	M1-Si	M2-Si
$f_e$ (%)	-	34.1	84.6
$f_r$ (%)	-	2.37	16.92
Water contact angle (°)			

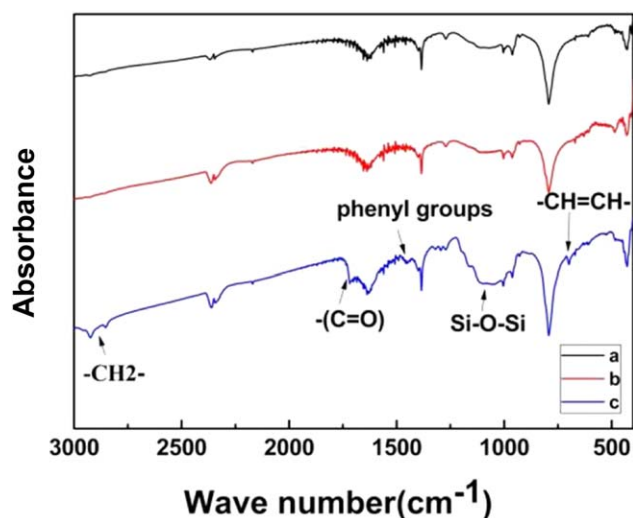
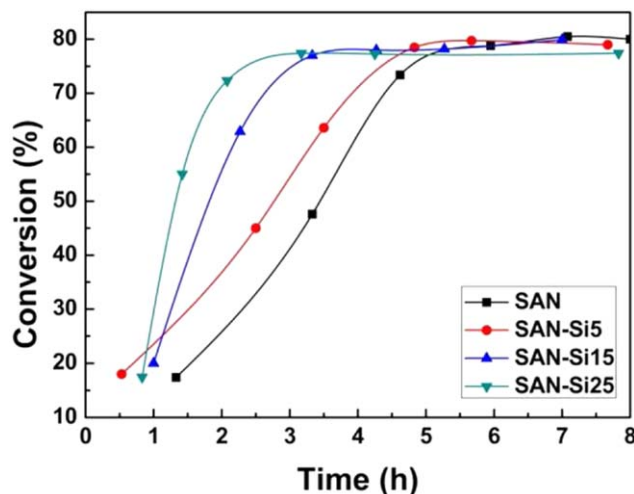
sulfate (0.02 g), sodium sulfate (0.2 g), and sodium nitrite (0.3 g). The final mixture was poured into the high-shear dispersing machine (ERS 2000/04, IKN® Equipment Shanghai Co., Ltd, Shanghai, China) to shear at 9000 rpm for 30 min. Finally, the copolymerization was performed at 70°C for 8 h under a slow stream of N<sub>2</sub>. The reaction was terminated by cooling the reaction system to room temperature. The conversion ratio of monomer to polymer was determined gravimetrically, according to<sup>36</sup>

$$C = \frac{M_2 - M_1 \times W_2}{M_1 \times W_1} \times 100\% \quad (3)$$

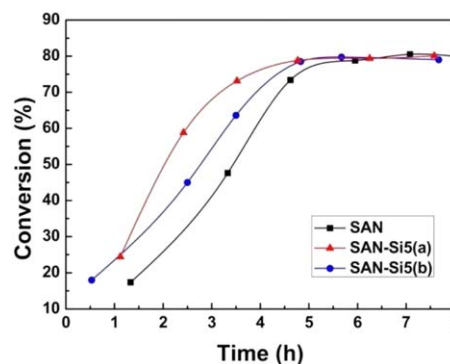
where  $C$  is the monomer conversion,  $M_1$  is the mass of the sample before drying,  $M_2$  is the mass of the sample after drying,  $W_1$  is the weight percentage of the monomers in the reaction, and  $W_2$  is the weight percentage of nonvolatile matter (such as PVA, BPO, TDM, TMPTS, nano-Si) in the reactor.

### Characterization

The Fourier transform infrared spectroscopy (FTIR; Thermo Nicolet Co., Ltd, Beijing, China) spectra of pristine nano-Si and modified nano-Si were recorded on a NEXUS-670 spectrometer in the range 400–4000 cm<sup>-1</sup> by using KBr pellets. The samples were prepared by grinding fine-grade KBr with 0.1 wt % of the sample. Water contact angle experiments of pristine nano-Si

**Figure 1.** FTIR spectra of (a) nano-Si, (b) M1-Si, and (c) M2-Si after Soxhlet extraction by toluene. [Color figure can be viewed in the online issue, which is available at wileyonlinelibrary.com.]**Figure 2.** Conversion–time curves for the microsuspension copolymerization of St and AN in the absence or presence of nano-Si modified by TMPTS and St. [Color figure can be viewed in the online issue, which is available at wileyonlinelibrary.com.]

and modified nano-Si were recorded on contact angle measurement equipment (JC2000A, Shanghai zhongchen Co., Ltd, Shanghai, China) by placing a water drop on the coating surface using a microsyringe. The scanning electron microscopy (SEM; Hitachi, Osaka, Japan) images of SAN and SAN-Si microspheres were observed on a JSM 6360LV (JEOL) apparatus. Energy dispersive spectroscopy (EDS; Hitachi, Osaka, Japan) was performed with an X-EDS GENESIS 2000XMS60 equipped on the SEM microscope. The transmission electron microscopy (TEM; Hitachi, Osaka, Japan) images were obtained with an HT7700 with an acceleration voltage of 100 kV. For TEM observation, the SAN-Si hybrid composite microspheres were placed on a 200-mesh carbon-coated copper grid. The thermogravimetric analysis (TGA; NETZSCH Germany Co., Ltd, Selb, Germany) experiments were performed on NETZSCH STA 409PC under a N<sub>2</sub> atmosphere from room temperature to 800°C at a heating rate of 10°C/min. The X-ray photoelectron spectroscopy (XPS;

**Figure 3.** Conversion–time curves for the microsuspension copolymerization between surface-modification methods and the presence or absence of nano-Si. SAN: prepared without nano-Si; SAN-Si5 (a) prepared with 5 wt % M1-Si; SAN-Si5 (b) prepared with 5 wt % M2-Si. [Color figure can be viewed in the online issue, which is available at wileyonlinelibrary.com.]

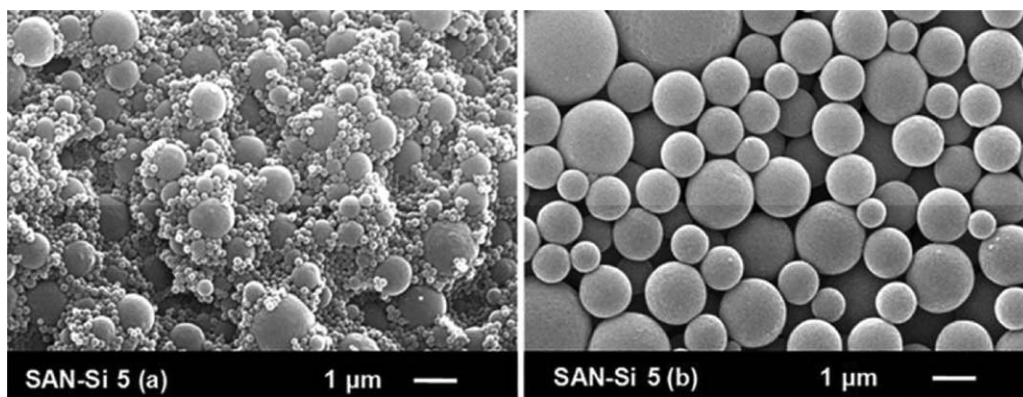


**Figure 4.** SEM images of SAN-Si5 prepared with different modified nano-Si: (a) M1-Si and (b) M2-Si.

ULVAC Japan Ltd, Chigasaki, Japan) experiments were carried out with an ESCA PHI 5000 Versa Probe spectrometer. The samples were attached to the spectrometer probe with double-sided adhesive tape and analyzed with monochromatized Al K $\alpha$  radiation (1486.6 eV). The base pressure inside the analysis chamber was maintained at  $1 \times 10^{-9}$  Torr. All binding-energy values were calculated relative to the C1s photoelectron peak at 285.0 eV. The survey scan was from 0 to 1200 eV to examine the atomic surface content.

## RESULTS AND DISCUSSION

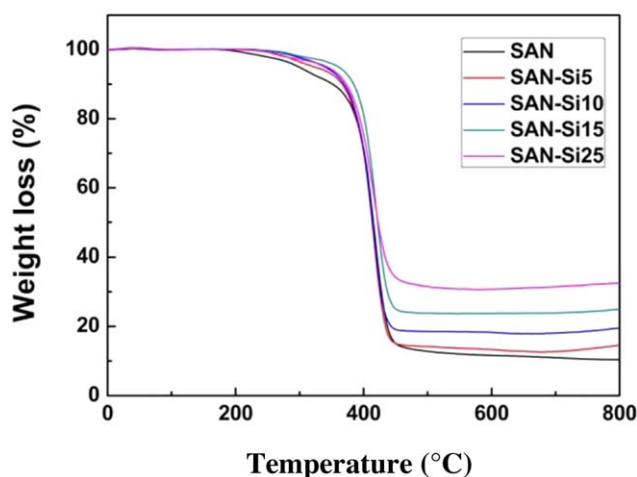
The influences of different methods for the surface modification of nano-Si on the grafting ratio ( $f_r$ ), grafting efficiency ( $f_e$ ), and the water contact angle of nano-Si are presented in Table I. The grafting ratio ( $f_r$ ) and efficiency ( $f_e$ ) of M1-Si (modified by mono-TMPTS) are much lower than those of M2-Si (modified by TMPTS and St).<sup>31</sup> The water contact angle of M1-Si is also lower than that of M2-Si, but both are higher than that of nano-Si. It can be inferred that TMPTS is not chemically bonded to the surface of nano-Si in the M1-Si sample because the measured water contact angle ( $58^\circ$ ) is almost the same as that of nano-Si ( $55^\circ$ ). While the M2-Si has achieved a higher

water contact angle ( $94^\circ$ ), this is ascribed to the formation of hydrophobic polymer layers chemically bonded to the surface of nano-Si. The main reason why TMPTS does not bond in the case of M1-Si is that mono-TMPTS is absorbed and wetted with difficulty on the surface of nano-Si. More hydrophobic oligomers formed by copolymerization of TMPTS and styrene more easily deposit onto the surface of nano-Si and then chemically bond to the surface of nano-Si by the hydrolysis and silanol-condensation reaction. Accordingly, in comparison with nano-Si modified by the mono-TMPTS, it can be known that nano-Si modified by TMPTS and St not only has a higher grafting ratio and efficiency, but also has a better hydrophobic property.

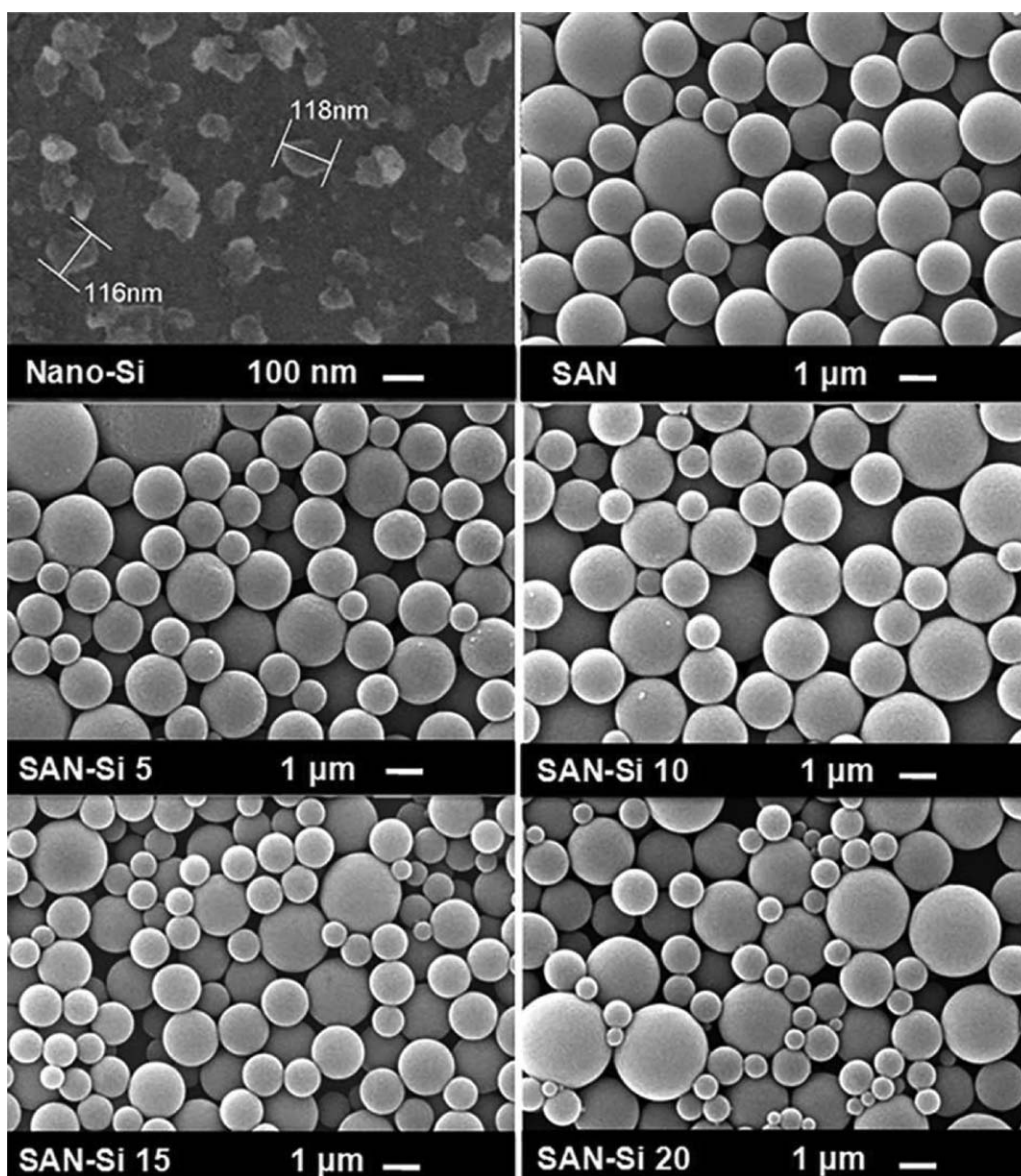
The FTIR spectra of pristine nano-Si and modified nano-Si are shown in Figure 1. The M1-Si after the Soxhlet extraction [Figure 1(b)] presents the same FTIR spectra of the pristine nano-Si [Figure 1(a)], which indicate mono-TMPTS could not be grafted onto the surface of nano-Si. From the FTIR spectra of the M2-Si shown in Figure 1(c), the absorption bands assigned to  $-\text{CH}_2-$  emerge at  $2937 \text{ cm}^{-1}$  and  $2852 \text{ cm}^{-1}$ , and the absorption bands located at  $1719 \text{ cm}^{-1}$ ,  $1485 \text{ cm}^{-1}$ , and  $700 \text{ cm}^{-1}$  are due to the vibration of  $-\text{C}=\text{O}$ , phenyl groups, and  $-\text{CH}=\text{CH}-$ , respectively. Moreover, the peak belonging to silane moieties (Si-O-Si stretching) in the range from  $1000$  to  $1100 \text{ cm}^{-1}$  becomes broader and stronger compared with the other two kinds of nano-Si, indicating the chemical bonding of TMPTS and St on the nano-Si surface. Thus, nano-Si modified by St and TMPTS is expected to disperse well in a SAN copolymer formed in a microemulsion polymerization.

Figure 2 shows the conversion versus time curves in the microemulsion copolymerization of St and AN with or without nano-Si modified by TMPTS and St. It can be observed that the polymerization rate increases with the increasing nano-Si dosage in the reaction system. The nano-Si causes a rapid increase in the overall rate of polymerization: the higher the dosage of nano-Si, the higher the monomer conversion rate under the same reaction time. The probably best reason is that the decomposition of the initiator is accelerated by the existence of nano-Si; the nano-Si seems to act as a redox in the polymerization reaction.

Figure 3 shows the comparison of conversion versus time curves between surface modification methods and the presence or



**Figure 5.** TGA curves of SAN and SAN-Si hybrid composite microspheres with various nano-Si contents. [Color figure can be viewed in the online issue, which is available at [wileyonlinelibrary.com](http://wileyonlinelibrary.com).]



**Figure 6.** SEM images of nano-Si, SAN, and SAN-Si hybrid composite microspheres with various nano-Si contents.

absence of nano-Si in the microsuspension copolymerization of St and AN. It is obvious that the polymerization rate with the M1-Si [SAN-Si5 (a)] shows a faster polymerization rate than the polymerization rate with M2-Si [SAN-Si5 (b)], and this indicates that the radical concentration in the M1-Si reaction system is higher than that in the M2-Si reaction system. Hence, the higher polymerization rate of SAN-Si5 [Figure 3(a)] is attributed to the larger quantity of the bare nano-Si in the M1-Si reaction system than that in the M2-Si reaction system for SAN-Si5 [Figure 3(b)]. It is considered that surface modification of nano-Si by mono-TMPTS is less effective on hydrophobic treatment, compared to nano-Si modified by TMPTS and St. The results are in good agreement with the experimental results of the grafting ratio and efficiency displayed in Table I.

Figure 4 shows the effect of two types of surface-modification methods on particle size and morphology of the SAN-Si5

composite microspheres corresponding to Figure 3. It is seen that the SAN-Si5 (a) hybrid composite microspheres prepared in the presence of M1-Si contain a lot of newly formed particles and larger particles. While SAN-Si5 (b) with M2-Si as the core mainly consists of larger particles, their particle size distribution is relatively broad. The formation of new particles in SAN-Si5 (a) is attributed to the emulsion polymerization of St and AN dissolved in the aqueous phase initiated by desorption of free radicals from composite particles. This is because the decomposition of the initiator is accelerated by the existence of the bare nano-Si. However, the new particles are not observed from the SEM image of SAN-Si5 (b), and it can be inferred that the surface of the M2-Si is covered with a more dense hydrophobic layer formed by TMPTS and St. Generally speaking, the nano-Si modified by TMPTS and St has a larger hydrophobic surface than that modified by TMPTS, so the M2-Si should become more compatible with polymer particles formed by the

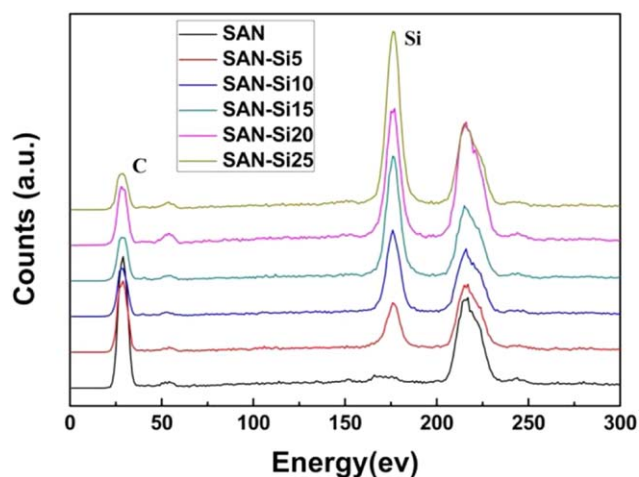


**Figure 7.** EDS of SAN and SAN-Si hybrid composite microspheres with various nano-Si contents. [Color figure can be viewed in the online issue, which is available at [wileyonlinelibrary.com](http://wileyonlinelibrary.com).]

microsuspension copolymerization of St and AN. Based on the experimental results above, it is more suitable to choose M2-Si to prepare the hybrid composite microspheres.

The thermal stabilities of SAN and SAN-Si hybrid composite microspheres are investigated by the TGA, and the results are illustrated in Figure 5. The weight of SAN slightly decreases at about 200°C, and the weight of SAN-Si hybrid composite microspheres starts to decrease at about 300°C, and this reveals the higher stability of SAN-Si hybrid composite microspheres. This is ascribed to the introduction of nano-Si. However, all of the microspheres degrade significantly at around 350°C and level off up to around 450°C. The degradation of the hybrid composite microspheres is mainly attributed to the decomposition of the polymer matrix.<sup>37</sup> The SAN copolymer with about 10 wt % residue is observed; namely, its carbon yield is about 10 wt %.<sup>38</sup> Furthermore, with the increase of nano-Si content, an increase in residual mass is observed, corresponding to about 15 wt %, 20 wt %, 25 wt %, and 35 wt % for SAN-Si5, SAN-

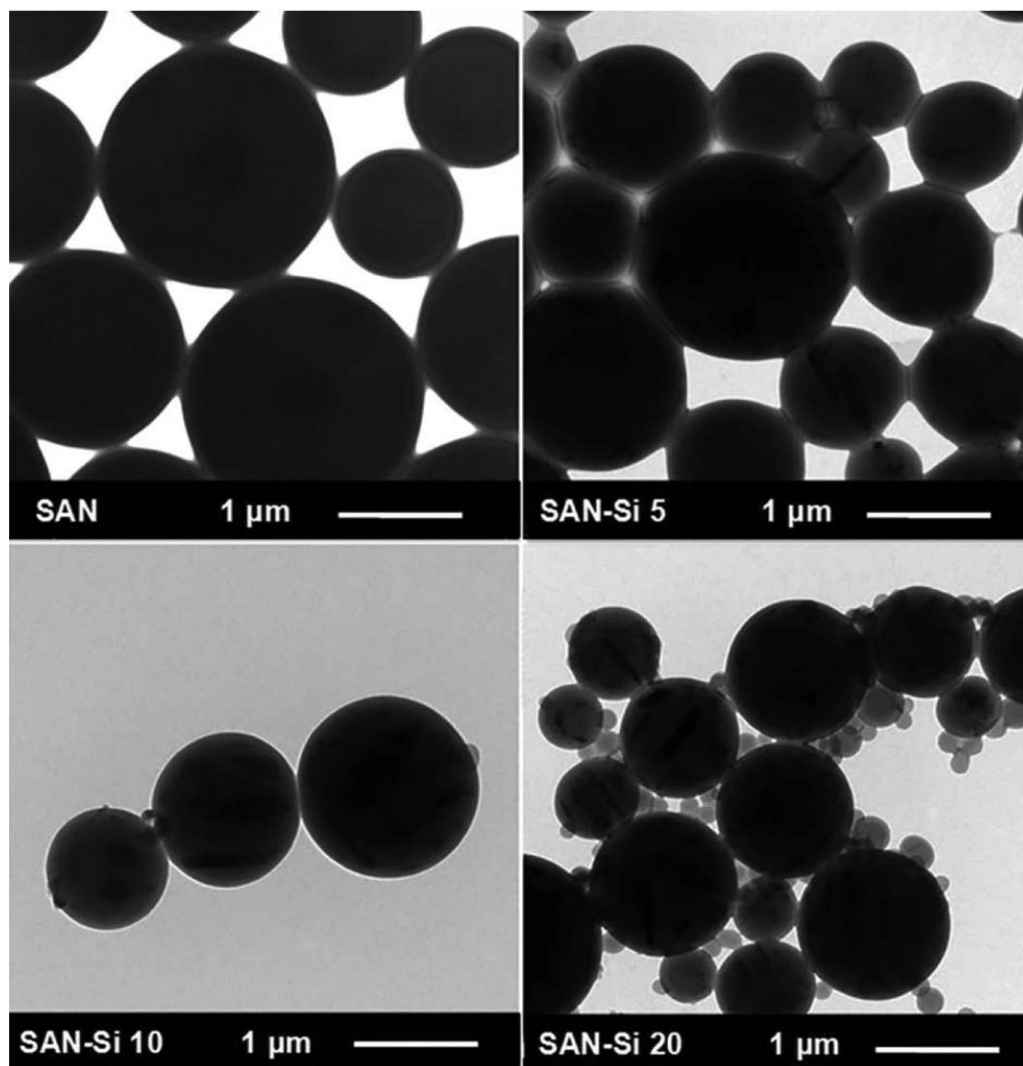


**Figure 8.** TEM images of SAN and SAN-Si hybrid composite microspheres with various nano-Si contents.

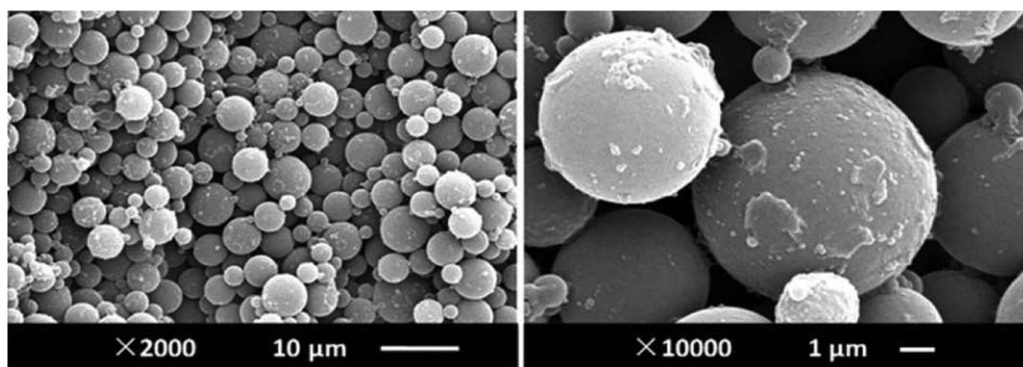


Figure 9. SEM images of SAN-Si25 with different magnifications.

Si10, SAN-Si15, and SAN-Si25, respectively. Therefore, it can be estimated that the corresponding content of the nano-Si inside the hybrid composite microspheres is about 5 wt %, 10 wt %, 15 wt %, and 25 wt %, respectively, which is consistent with the feeding ratio of the nano-Si.

SEM and TEM analyses are used in an effort to explore the surface morphology and nano-Si distribution within the hybrid composite microspheres. The SEM micrographs of nano-Si, SAN, and SAN-Si hybrid composite microspheres are illustrated in Figure 6. As shown in Figure 6, the nano-Si exhibits irregular nanoflakes of about 60–150 nm, obtained by the fracturing of the commercial micrometric silicon powder by the high-energy wet ball milling.<sup>29</sup> From the SEM images (Figure 6) of SAN and SAN-Si composite microspheres with various nano-Si contents, all samples show a relatively smooth spherical morphology with a large size distribution, and no bare nano-Si is observed on the surface of these microspheres. These apparent characteristics imply that the nano-Si has been well encapsulated in the SAN. In addition, it is noticed that the particle size distributions of SAN-Si hybrid composite microspheres become broader with increasing nano-Si content, even though there is no big difference in the surface morphology. The reason for this change in

the particle size distribution is not clear, and more work is needed. With this end in view, EDS is employed to verify nano-Si contents in the hybrid composite microspheres, and the results are shown in Figure 7. The Si peak intensity increases in proportion to the increasing nano-Si content, suggesting that the nano-Si can be completely encapsulated into the SAN copolymer.

The TEM micrographs of SAN and SAN-Si microspheres with various nano-Si contents are shown in Figure 8. The SAN-Si hybrid composite microspheres, similar to SAN particles, are found to be comparatively smooth and spherical in shape with a broad size distribution and containing many irregular darker areas, which are nano-Si. The nano-Si encapsulated inside the SAN-Si hybrid composite microspheres is randomly distributed. Moreover, the darker areas in the microspheres become denser with increasing nano-Si content, and there is no free nano-Si outside the hybrid composite microspheres. A lot of smaller microspheres appear as the nano-Si contents increase. These results are consistent with the SEM analysis. Therefore, it is feasible to prepare the hybrid composite microspheres with uniformly distributed nano-Si encapsulated in SAN by the micro-suspension polymerization.

The SEM images of SAN-Si25 with various magnifications are presented in Figure 9. It is obvious that the surface of the hybrid composite microspheres becomes rough and uneven, and a part of the nano-Si transfers onto the surface of the hybrid composite microspheres. Compared with other hybrid composite microspheres with lower nano-Si contents (Figure 6), the average particle diameter of SAN-Si25 becomes exceptionally larger. Moreover, the surface silicon content of SAN-Si hybrid composite microspheres with various nano-Si contents is displayed in Figure 10.

The surface atomic concentration of SAN-Si5 to SAN-Si20 slightly increases with increasing nano-Si contents. When the nano-Si contents increase up to 25 wt %, the nano-Si atomic concentration on the surface significantly increases. It indicates that more nano-Si emerges on the surface of SAN-Si25 hybrid composite microspheres. Therefore, the nano-Si will transfer onto the surface of the microspheres in the emulsification process and act as an inorganic dispersant,<sup>39</sup> which is consistent with the SEM analysis (Figure 9).

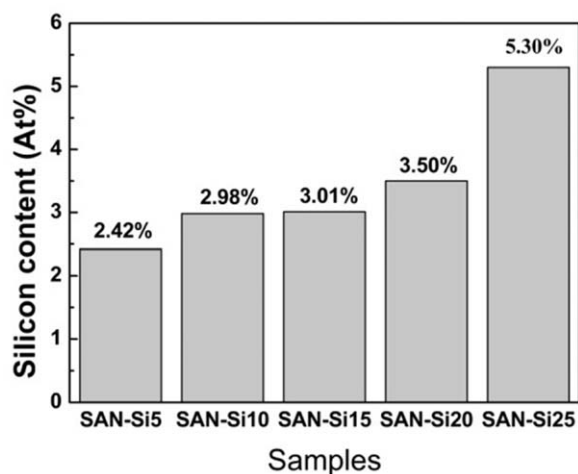


Figure 10. The surface silicon content of SAN-Si hybrid composite microspheres with various nano-Si contents.

## CONCLUSIONS

The SAN-Si hybrid composite microspheres were successfully prepared via microsuspension polymerization in the presence of nano-Si obtained by high-energy wet ball milling. Hydrophilic nano-Si needs to be pretreated before encapsulation. The nano-Si modified by TMPTS and St was covered with a more dense, hydrophobic coating layer compared with the mono-TMPTS modified nano-Si, and it has a small effect on the copolymerization of St and AN during the microsuspension polymerization process. The nano-Si contents greatly affect the polymerization rate: the higher the nano-Si content, the faster the polymerization rate. The thermostability of the SAN-Si hybrid composite microspheres is better than that of SAN without nano-Si. Furthermore, the nano-Si could be entirely encapsulated into the SAN copolymer when the loading amount is lower than 20 wt %. However, the nano-Si may overflow from the inner core to the outside surface in the emulsification process and act as an inorganic dispersant once the nano-Si contents in the hybrid composite microspheres reach 25 wt %.

## REFERENCES

- Chen, Z.; Christensen, L.; Dahn, J. R. *J. Appl. Polym. Sci.* **2004**, *91*, 2958.
- Cai, J.; Zuo, P.; Cheng, X.; Xu, Y.; Yin, G. *Electrochem. Commun.* **2010**, *12*, 1572.
- Chen, D.; Yi, R.; Chen, S.; Xu, T.; Gordin, M. L.; Wang, D. *Solid State Ionics* **2014**, *254*, 65.
- Wang, H.; Shu, L.; Jiang, S. *J. Appl. Polym. Sci.* **2010**, *117*, 2790.
- Vital, A.; Richter, J.; Figi, R.; Nagel, O.; Aneziris, C. G.; Bernardi, J.; Graule, T. *Ind. Eng. Chem. Res.* **2007**, *46*, 4273.
- Cui, L.; Hu, L.; Choi, J. W.; Cui, Y. *ACS Nano* **2010**, *4*, 3671.
- Nguyen, S. H.; Lim, J. C.; Lee, J. K. *Electrochim. Acta* **2012**, *74*, 53.
- Laïk, B.; Eude, L.; Pereira-Ramos, J. P.; Cojocar, C. S.; Pribat, D.; Rouvière, E. *Electrochim. Acta* **2008**, *53*, 5528.
- Chan, C. K.; Patel, R. N.; O'Connell, M. J.; Korgel, B. A.; Cui, Y. *ACS Nano* **2010**, *4*, 1443.
- Liu, J.; Li, N.; Goodman, M. D.; Zhang, H.; Epstein, E. S.; Huang, B.; Pan, Z.; Kim, J.; Choi, J. H.; Huang, X.; Liu, J.; Hsia, K. J.; Dillon, S. J.; Braun, P. V. *ACS Nano* **2015**, *9*, 1985.
- Yin, Y.; Xin, S.; Wan, L. J.; Li, C. J.; Guo, Y. G. *J. Phys. Chem. C* **2011**, *115*, 14148.
- Zhang, F.; Yang, X.; Xie, Y.; Yi, N.; Huang, Y.; Chen, Y. *Carbon* **2015**, *82*, 161.
- He, M.; Sa, Q.; Liu, G.; Wang, Y. *ACS Appl. Mater. Interfaces* **2013**, *5*, 11152.
- Si, Q.; Matsui, M.; Horiba, T.; Yamamoto, O.; Takeda, Y.; Seki, N.; Imanishi, N. *J. Power Sources* **2013**, *241*, 744.
- Hasegawa, T.; Mukai, S. R.; Shirato, Y.; Tamon, H. *Carbon* **2004**, *42*, 2573.
- Hu, Y. S.; Demir-Cakan, R.; Titirici, M. M.; Muller, J. O.; Schlogl, R.; Antonietti, M.; Maier, J. *Angew. Chem.* **2008**, *47*, 1645.
- Wang, H.; Wu, P.; Shi, H.; Lou, F.; Tang, Y.; Zhou, T.; Zhou, Y.; Lu, T. *Mater. Res. Bull.* **2014**, *55*, 71.
- Ng, S.; Wang, J.; Wexler, D.; Chew, S. Y.; Liu, H. K. *J. Phys. Chem. C* **2007**, *111*, 11131.
- Wang, Z.; Tonderys, D.; Leggett, S. E.; Williams, E. K.; Kiani, M. T.; Spitz Steinberg, R.; Qiu, Y.; Wong, I. Y.; Hurt, R. H. *Carbon* **2016**, *97*, 14.
- Li, J.; Li, L.; Zhang, B.; Yu, M.; Ma, H.; Zhang, J.; Zhang, C.; Li, J. *Ind. Eng. Chem. Res.* **2014**, *53*, 13348.
- Thakur, M.; Pernites, R. B.; Nitta, N.; Isaacson, M.; Sinsabaugh, S. L.; Wong, M. S.; Biswal, S. L. *Chem. Mater.* **2012**, *24*, 2998.
- Wu, H.; Yu, G.; Pan, L.; Liu, N.; McDowell, M. T.; Bao, Z.; Cui, Y. *Nat. Commun.* **2013**, *4*, 1943.
- Liu, G.; Xun, S.; Vukmirovic, N.; Song, X.; Olalde-Velasco, P.; Zheng, H.; Battaglia, V. S.; Wang, L.; Yang, W. *Adv. Mater.* **2011**, *23*, 4679.
- Ebrahimpour, O.; Esmaili, B.; Griffon, L.; Chaouki, j.; Dubois, C. *J. Appl. Polym. Sci.* **2014**, *131*, 40425.
- Zhang, T.; Fu, L.; Gao, J.; Yang, L.; Wu, Y.; Wu, H. *Pure Appl. Chem.* **2006**, *78*, 1889.
- Zhang, H.; Xu, L.; Yang, F.; Geng, L. *Carbon* **2010**, *48*, 688.
- Mdletshe, T. S.; Mishra, S.; Mishra, A. K. *J. Appl. Polym. Sci.* **2015**, *132*, 42145.
- Kwon, E.; Lim, H. S.; Sun, Y. K.; Suh, K. D. *Solid State Ionics* **2013**, *237*, 28.
- Zhang, M.; Hou, X.; Wang, J.; Li, M.; Hu, S.; Shao, Z.; Liu, X. *J. Alloys Compd.* **2014**, *588*, 206.
- de Alcantara Abdala, J. M.; Fernandes, B. B.; dos Santos, D. R.; Rodrigues Henriques, V. A.; de Moura Neto, C.; Ramos, A. S. *J. Alloys Compd.* **2010**, *495*, 423.
- Chen, T.; Cao, Z.; Guo, X.; Nie, J.; Xu, J.; Fan, Z.; Du, B. *Polymer* **2011**, *52*, 172.
- Pla, F.; Fonteix, C.; Van der Wal, H. *Chem. Eng. Technol.* **2010**, *33*, 1859.
- Shi, J.; Bao, Y.; Huang, Z.; Weng, Z. *J. Zhejiang Univ., Sci.* **2004**, *5*, 709.
- Nakai, S.; Akiyoshi, M.; Okubo, M. *J. Appl. Polym. Sci.* **2013**, *127*, 2407.
- Abdollahi, M.; Alamdari, P.; Koolivand, H.; Ziaee, F. *J. Polym. Res.* **2013**, *20*, 239.
- Betancourt-Galindo, R.; Cabrera Miranda, C.; Puente Urbina, B. A.; Castañeda-Facio, A.; Sánchez-Valdés, S.; Mata Padilla, J.; García Cerda, L. A.; Perera, Y. A.; Rodríguez-Fernández, O. S. *ISRN Nanotechnol.* **2012**, *2012*, 1.
- Mallakpour, S.; Barati, A. *Prog. Org. Coat.* **2011**, *71*, 391.
- Partouche, E.; Margel, S. *Carbon* **2008**, *46*, 796.
- Duan, L.; Chen, M.; Zhou, S.; Wu, L. *Langmuir* **2009**, *25*, 3467.